LETTER • OPEN ACCESS

Catchment precipitation partitioning in the Budyko framework is controlled by root zone storage capacity

ENVIRONMENTAL RESEARCH
LETTERS

OPEN ACCESS

RECEIVED
4 July 2025

REVISED
27 March 2026

ACCEPTED FOR PUBLICATION
17 April 2026

PUBLISHED
5 May 2026

LETTER

Catchment precipitation partitioning in the Budyko framework is controlled by root zone storage capacity

Muhammad Ibrahim[1,*], **Fransje van Oorschot**[2], **Ruud van der Ent**[1], **Markus Hrachowitz**[1] and **Miriam Coenders-Gerrits**[1]

[1] Department of Water Management, Faculty of Civil Engineering and Geosciences, Delft University of Technology, Delft, The Netherlands
[2] Drents Overijsselse Delta Water Board, Zwolle, The Netherlands
[*] Author to whom any correspondence should be addressed.

E-mail: m.ibrahim@tudelft.nl

Keywords: root zone storage capacity, Budyko framework, precipitation partitioning, Fu's equation

Supplementary material for this article is available online

Abstract

Quantification of long-term partitioning of precipitation into evaporation and runoff is a fundamental pursuit in catchment hydrology. The Budyko framework provides a theoretical basis for this and estimates the evaporative fraction based on the aridity index. However, deviations from the global-average Budyko curve point to additional controls on precipitation partitioning beyond the aridity index. We hypothesized that root zone storage capacity ($S_{r,\max}$), defined as maximum subsurface water volume accessible to vegetation roots, is a key driver of these deviations. The relationship between $S_{r,\max}$ and precipitation partitioning in the Budyko space was investigated globally across >5000 catchments. $S_{r,\max}$ was calculated using the memory method based on runoff observations and the water balance. The ω-parameter from Fu's equation, which was used here to construct parametric Budyko curves, reflects deviations from the global-average Budyko curve and hence precipitation partitioning. Results revealed a globally stronger correlation (Spearman's $\rho = 0.68$) of ω with $S_{r,\max}$, than with other potential controls, indicating $S_{r,\max}$ as a dominant driver of precipitation partitioning. Further analysis based on Köppen–Geiger climatic zone classification revealed variations in the $S_{r,\max}$–ω relationship, with the strongest correlations observed in cold ($\rho = 0.87$) and Mediterranean ($\rho = 0.83$) climates, followed by temperate ($\rho = 0.76$), tropical ($\rho = 0.64$) and arid climates ($\rho = 0.61$). Regional differences in $S_{r,\max}$ indicate that, at a given aridity, E_A/P largely reflects vegetation adaptation to the seasonal interplay between water supply and atmospheric water demand. This study provides strong empirical evidence on a global scale for $S_{r,\max}$ as a governing factor in modulating catchment precipitation partitioning, as evident in the Budyko space. As a major implication our results provide a theoretical basis for the maximum values of $S_{r,\max}$ found in nature, as constrained by the water and energy limits of the Budyko framework.

1. Introduction

The partitioning of precipitation (P) into evaporation (E_A) and runoff (Q) is a fundamental characteristic of terrestrial hydrological systems, representing the exchange of water and energy fluxes between the subsurface and atmosphere. As such, robust quantification of this long-term average partitioning at the catchment scale is crucial for many hydrological applications. Over the past century, several non-parametric empirical–analytical models, commonly referred to as Budyko curves, have been developed to describe this partitioning (Schreiber 1904, Oldekop 1911, Budyko 1948, Turc 1954). These models relate long-term average potential evaporation ($\overline{E_P}$) and precipitation ($\bar{P}$), via the aridity index $\overline{I_A} = \overline{E_P}/\bar{P}$, to the evaporative index $\overline{I_E} = \overline{E_A}/\bar{P}$ of a catchment. Since then, the Budyko framework has been demonstrated

in a vast number of studies to broadly describe hydrological partitioning pattern across a wide and diverse range of climatic conditions (Milly 1994, Zhang *et al* 2001, Gentine *et al* 2012, Shao *et al* 2012, Xu *et al* 2013, Berghuijs *et al* 2014).

While non-parametric Budyko curves capture global average partitioning patterns, individual catchments often deviate from these averages (Donohue *et al* 2007, Jaramillo *et al* 2022, Reaver *et al* 2022, Ibrahim *et al* 2025a). To account for these deviations, several functionally equivalent parametric reformulations of the Budyko curves have been developed (Turc 1954, Mezentsev 1955, Tixeront 1964, Fu 1981) by introducing a catchment-specific parameter, hereafter referred to as ω [-]. The ω-parameter encapsulates integrated catchment characteristics that influence water storage and release, beyond what is explained by I_A (Milly 1994, Zhang *et al* 2004, Donohue *et al* 2012, Shao *et al* 2012). While the ω-parameter has enhanced our ability to describe hydrological behaviour of catchments, its physical interpretation remains challenging. As a process-agnostic parameter, statistically derived to fit observations, ω lacks a clear physical meaning, and the factors controlling it and thus precipitation partitioning, are not well understood. Multiple factors that may influence ω and thus precipitation partitioning have previously been proposed, including rainfall seasonality (Milly 1994, Porporato *et al* 2004, Potter *et al* 2005, Padrón *et al* 2017), fraction of snow (Berghuijs *et al* 2014), vegetation (Zhang *et al* 2001, Porporato *et al* 2004, Donohue *et al* 2012, Gentine *et al* 2012, Sterling *et al* 2012, Williams *et al* 2012, Li *et al* 2013, Xu *et al* 2013, Zhou *et al* 2015, Daly *et al* 2019), reservoirs and irrigation practices (Wang and Hejazi 2011, Jaramillo and Destouni 2015) as well as groundwater import/export (Bouaziz *et al* 2018).

Among the potential factors controlling the ω-parameter, the role of vegetation and specifically, the role of vegetation accessible soil water storage in modulating precipitation partitioning has received particular attention. Milly (1993) introduced a stochastic soil moisture model linking soil water storage dynamics to evaporation and runoff within the Budyko framework, emphasizing the role of subsurface water in modulating the catchment hydrological responses. Building on the work of Laio *et al* (2001), Porporato *et al* (2004) incorporated vegetation dynamics by explicitly considering rooting depth and soil moisture feedbacks into their eco-hydrological model, detailing how variations in soil water storage and precipitation influence partitioning. Their theoretical-stochastic model suggests that increased vegetation accessible soil water storage increases ω and consequently I_E. These findings have since been complemented by empirical studies. For example, Gentine *et al* (2012), using data of ∼400 US catchments, inverted the Budyko curve to show how rooting depths adapt to I_A and rainfall seasonality, thereby regulating the surface water balance. Similarly, Donohue *et al* (2012) investigated the role of rooting depth, storm depth and soil water storage for Australian catchments by combining the models of Porporato *et al* (2004) and Choudhury (1999), identifying rooting depth as a key factor in modulating catchment responses, and improving runoff predictions in humid catchments. Yet, Daly *et al* (2019), emphasized challenges in applying such models to more heterogenous catchments.

However, Padrón *et al* (2017) offered a contrasting perspective suggesting that several vegetation related indices, including vegetation accessible soil water storage, play only a minor role in controlling ω. These studies identifying vegetation accessible soil water storage as a dominant control on ω, and thus on precipitation partitioning, are either theoretical or based on rather small empirical samples limited to the US and Australia. It therefore remains unclear whether and where the overall findings of these studies can be assumed to hold across a wider spectrum of catchments with more diverse climatic and landscape characteristics and why Padrón *et al* (2017) observed a limited vegetation influence.

The objective of this study is therefore to systematically evaluate the role of vegetation accessible soil water storage in controlling ω and associated precipitation partitioning, using a large global sample of catchments spanning diverse climates and landscapes. We defined vegetation accessible soil water storage as the maximum water volume that can be held in the pore spaces of subsurface between field capacity and permanent wilting point within the reach of plant roots. As such, it represents the water reservoir available to vegetation to meet evaporation demands during dry periods, thereby controlling P partitioning.

Building on the foundational work of Porporato *et al* (2004) and Gentine *et al* (2012), we estimate catchment-scale vegetation accessible soil water storage, hereafter referred to as root zone storage capacity ($S_{r,\max}$), based on the memory method (van Oorschot *et al* 2021). As a functionally similar, simplified version of the method used by Gentine *et al* (2012), it has been demonstrated to provide robust estimates of $S_{r,\max}$ based on water balance data in a wide range of environments (Gao *et al* 2014, de Boer-Euser *et al* 2016, Nijzink *et al* 2016, Bouaziz *et al* 2020, Hrachowitz *et al* 2021, Wang *et al* 2024, van Oorschot *et al* 2024a, 2024b). More specifically, relating these $S_{r,\max}$ estimates to ω for >5000 river catchments worldwide, we test the hypothesis that $S_{r,\max}$ is globally a dominant control on ω and, by extension, on catchment precipitation partitioning.

2. Datasets and methods

2.1. Hydrological and meteorological data

Mean annual observed streamflow data were obtained from GSIM (Do *et al* 2018, Gudmundsson *et al* 2018), Caravan (Kratzert *et al* 2023), ADHI (Tramblay *et al* 2021) and the mountainous rivers data of Central Asia (Marti *et al* 2023). Daily precipitation P and temperature T were obtained from the bias-corrected GSWP-3 reanalysis dataset (0.5 × 0.5; 1981–2010) (Dirmeyer *et al* 2006). Although not direct observations, GSWP-3 is widely used in global hydrological studies (Ghiggi *et al* 2019, Stacke and Hagemann 2021, Hou *et al* 2022) and provides a harmonized dataset essential for analysing >5000 catchments across diverse climates. Potential evaporation E_P was estimated using the Hargreaves and Samani (1982) method, which assumes a well-watered reference surface without vegetation type adjustment. While simplified, it provides consistent input across all catchments. Bi-weekly NDVI (0.083 × 0.083; 1982–2010) and annual land use were obtained from NASA ESDIS (Pinzon *et al* 2023) and HILDA + (Winkler *et al* 2021), respectively. Catchment-average *P, T,* NDVI, and LU were extracted using weighted area means and bilinear interpolation. The precipitation seasonality index (I_S) of effective precipitation (P_e) i.e. liquid precipitation plus snowmelt, was determined following Gao *et al* (2014). High I_S values suggest large fractions of annual precipitation falling in short periods; low I_S indicates a more uniform yearly distribution. Catchments were classified into five climate zones using the Köppen–Geiger climate zones (Beck *et al* 2018): cold, Mediterranean, temperate, tropical, and arid. Details of all catchment-related variables are provided in table 1.

From the available catchments with streamflow data, 5717 were selected based on four criteria: (1) ⩾20 years of data between 1981–2010; (2) no 'Caution' data quality flag; (3) catchment area <10 000 km^2 to limit heterogeneity; (4) no water balance deficit, i.e. $\bar{P} - \bar{Q} < 0$, indicating major data errors. The selected catchments represent diverse topographic and hydro-climatic conditions (figure 1), with areas from 0.1 to 9975 km^2 (median ∼630 km^2; figure 1(f)), mean elevations from 7 to 4789 m (median ∼485 m; figure 1(g)), long-term average aridity indices ($\overline{I_A}$) from 0.15 to 11 (median: 1.01; figure 1(c)) and evaporative indices ($\overline{I_E}$) from 0.09 to 1 (median: 0.66; figure 1(b)). High I_S values are observed in central and western Canada, northern India, and northeastern Brazil (figure 1(d)). The study catchments are scattered across climatic zones (figure 1(h)), with most located in cold (∼33%) and temperate regions (∼36%).

2.2. Methods

2.2.1. Estimation of ω-parameter

To investigate the relationship between the ω-parameter and root zone storage capacity $S_{r,\max}$ as well as other variables listed in table 1, we calculated ω for each catchment using the Tixeront–Fu reformulation of the Budyko hypotheses (Tixeront 1964, Fu 1981, Zhang *et al* 2004). Higher ω indicates a higher $\overline{E_A}/\bar{P}$ for a given $\overline{E_P}/\bar{P}$, although the relationship is non-linear, with sensitivity decreasing as ω increases (Zhang *et al* 2004). Greve *et al* (2015) report a global average ω of ∼2.6

$$\frac{\overline{E_A}}{\bar{P}} = 1 + \frac{\overline{E_P}}{\bar{P}} - \left[1 + \left(\frac{\overline{E_P}}{\bar{P}}\right)^{\omega}\right]^{\frac{1}{\omega}} \quad (1)$$

where $\overline{E_A}$ is actual evaporation calculated from the long-term mean water balance $\overline{E_A} = \bar{P} - \bar{Q} - \mathrm{d}S/\mathrm{d}t$, assuming negligible long-term storage change ($\mathrm{d}S/\mathrm{d}t = 0$) over >20 years. This assumption is reasonable for large sample studies as Han *et al* (2020) demonstrated that ∼80% of catchments reach steady state within 20 years and only 6% within >30 years. Although it may not hold in catchments with significant inter-basin groundwater flow, glacier influence or long-term (aquifer) depletion, it is widely applied in large-sample studies (e.g. Fu (1981), Zhang *et al* (2004), Greve *et al* (2015), Mianabadi *et al* (2020), Li and Quiring (2022)) as errors are likely to cancel across large spatial samples. A study by Ibrahim *et al* (2025a) supports this assumption. They found that systematic shifts in the long-term water balance, indicative of $\mathrm{d}S/\mathrm{d}t \neq 0$, are rare as only ∼4% of 2387 global catchments show trend-like behaviour over multiple decades.

2.2.2. Estimation of root zone storage capacity $S_{r,max}$

Direct observations of $S_{r,\max}$ and rooting systems are scarce and generally unavailable at the catchment scale, and integrating them at this scale is challenging due to landscapes heterogeneity (de Boer-euser *et al* 2016, Hrachowitz *et al* 2021). Here, we estimate $S_{r,\max}$ using the memory method, which robustly estimates catchment-scale root zone storage capacity by relying on annual maximum water storage deficits (S_d) per year, estimated as daily cumulative deficit from daily observed hydro-climatic data, i.e. effective precipitation P_e (liquid precipitation input plus snowmelt), potential evaporation and runoff (Gao *et al* 2014, Hrachowitz *et al* 2021, van Oorschot *et al* 2024a, 2024b). The P_e that contributes to S_d is derived from a simple water balance model that accounts for interception (S_i) and snow storages (S_{snow}), which regulate partitioning of total P into throughfall and snowmelt (M_{snow}), and thus liquid water infiltrating into

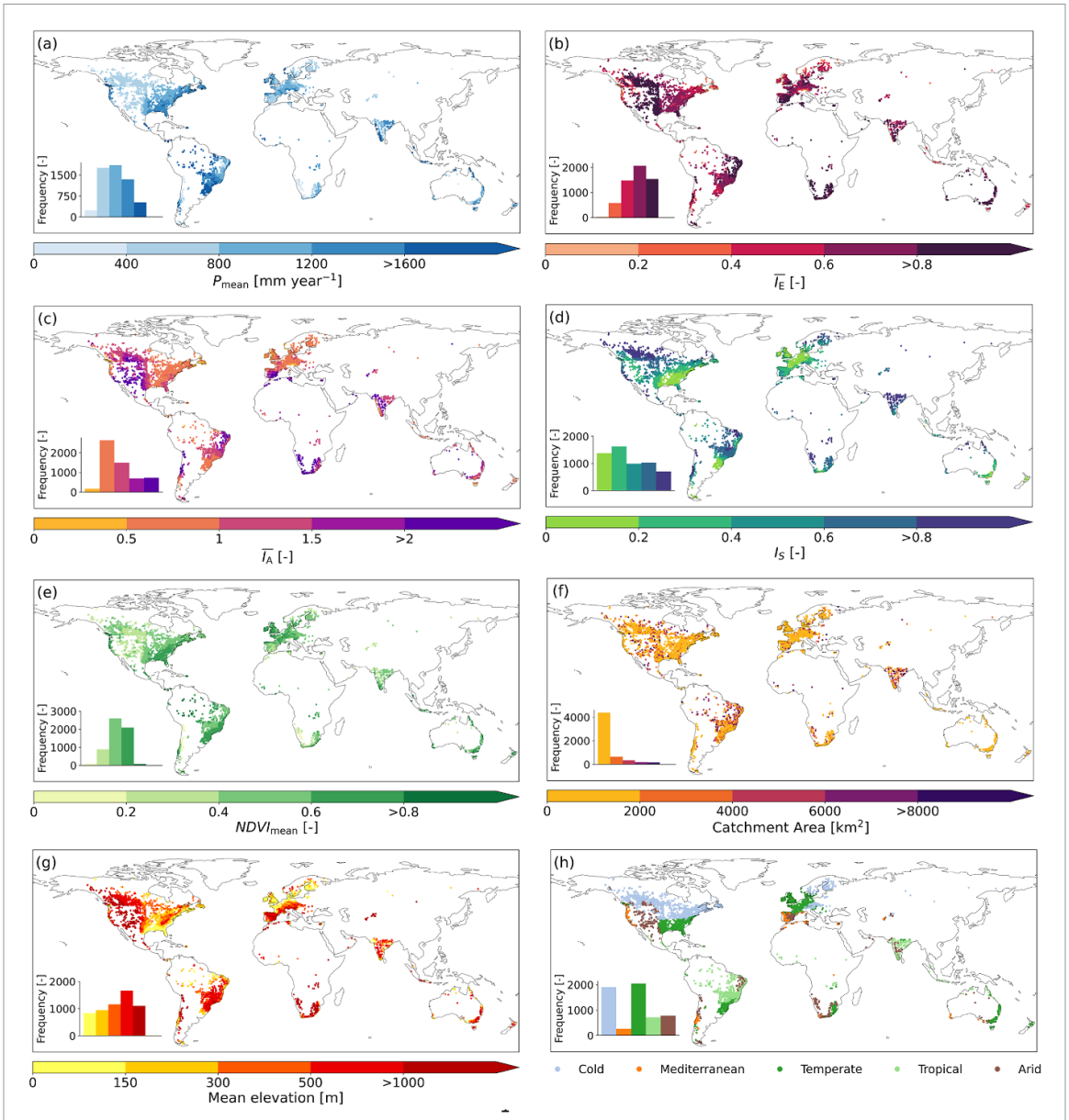

Figure 1. Distribution of the 5717 study catchments along with associated long term mean (1981–2010) hydro-climatological indices and topographic characteristics: (a) precipitation P, (b) evaporative index $\overline{I_E} = \overline{E_A}/\overline{P}$, (c) Aridity Index $\overline{I_A} = \overline{E_P}/\overline{P}$, (d) seasonality index of effective precipitation I_S, (e) NDVI, (f) catchment area, (g) mean elevation, and (h) climatic zones used in this study (based on Köppen–Geiger): cold (Dfa, Dfb, Dfc), Mediterranean (Csa, Csb), temperate (Cwa, Cwb, Cfa, Cfb), tropical (Af, Am, Aw), and arid (BWh, BWk, BSh, BSk).

the soil. Interception evaporation (E_i) is subtracted from S_i and remaining water, together with snowmelt infiltrates the root zone, from where E_A is calculated (figure 2(a)). The resulting annual maximum storage deficits (S_d) represent the volume of water that has in the past been available and accessible to the roots of vegetation to fulfil transpiration needs during dry periods.

$S_{r,max}$ was estimated by fitting a Gumbel distribution to the annual maximum S_d series, assuming vegetation develop root systems to cope with dry spells with a ∼20 year return period (Gao *et al* 2014, Nijzink *et al* 2016, Bouaziz *et al* 2020, Hrachowitz *et al* 2021). This method assumes that vegetation has adapted its $S_{r,max}$ to buffer hydroclimatic seasonality by creating sufficient storage to sustain itself during dry periods (Donohue *et al* 2012, Gentine *et al* 2012, Gao *et al* 2014, de Boer-euser *et al* 2016, Nijzink *et al* 2016, Wang-Erlandsson *et al* 2016, Bouaziz *et al* 2020, Dralle *et al* 2020, Hrachowitz *et al* 2021).

Potential evaporation (E_P) from the Hargreaves–Samani method, lacking vegetation-specific adjustment, is merely used as seasonal scaling for the long-term mean E_A from the water balance, and thus brings in the seasonal aspect of atmospheric demand rather than its absolute magnitude. Doubling E_P would not change the $S_{r,max}$ estimate, since the

Table 1. List of the variables used in the study in addition to $S_{r,\max}$ to explore relationships with ω along with their symbols, units and associated data sources or methodological references. Methodological references are shown in italics to distinguish them from data sources.

Variable name	Symbol	Units	Data source or *methodological reference*
	Hydro-meteorological variables		
Precipitation	P	mm d^{-1}	Global soil wetness project phase-3 (GSWP-3) (Dirmeyer *et al* 2006)
Streamflow	$\bar{Q}$	mm d^{-1}	Global Streamflow indices and metadata (GSIM) archive (Do *et al* 2018, Gudmundsson *et al* 2018) Caravan (Kratzert *et al* 2023) African database of hydrometric indices (ADHI) (Tramblay *et al* 2021) Central Asia -Discharge (Marti *et al* 2023)
Temperature	T	°C	Global soil wetness project phase-3 (GSWP-3) (Dirmeyer *et al* 2006)
Potential evaporation	E_P	mm d^{-1}	Hargreaves and Samani (1982)
Seasonality index of effective precipitation (Liquid precipitation input + snowmelt)	I_S	[-]	Gao *et al* (2014)
Fraction of snow (as part of total precipitation)	F_{Snow}	%	*Based on threshold temperature* $T_t = 0$ °C (van Oorschot *et al* 2024b)
	Vegetation-related variables		
Long-term mean normalized difference vegetation index	NDVI	[-]	Pinzon *et al* (2023)
Long-term mean fraction of forest cover	F_{Forest}	%	HILDA + (Winkler *et al* 2021)
Long-term mean fraction of sparse vegetation cover	F_{Sparse}	%	HILDA + (Winkler *et al* 2021)
Long-term mean fraction of mixed (urban + cropland + pasture + shrubland) landcovers	F_{UCPS}	%	HILDA + (Winkler *et al* 2021)
Fraction of irrigation area	$F_{Irrigation}$	%	Siebert *et al* (2015)
	Soil-related variables		
Plant extractable soil water content	PESWC	mm	Dunne and Willmott (2000)
Potential storage of water derived from soil texture	PSWST	mm	Webb *et al* (2000)
Fraction of clay	F_{Clay}	%	Hengl *et al* (2017)
Fraction of sand	F_{Sand}	%	Hengl *et al* (2017)

storage requirement is constrained by precipitation and runoff. Vegetation effects on E_A are indirectly captured via observed precipitation and streamflow, which together constrain the root zone storage estimates. Consequently, $S_{r,\max}$ reflects the integrated water available to vegetation at the catchment scale, with limited sensitivity to absolute E_P magnitude. Importantly, this also means that in heterogeneous catchments, $S_{r,\max}$ represents a catchment-scale property averaged over different vegetation types and land covers, which is sufficient for the catchment-scale focus of this study. A schematic is shown in figure 2; equations in supplementary section S1 and a detailed description can be found in van Oorschot *et al* (2024b).

Given the expected monotonic but potentially non-linear relationships between ω and $S_{r,\max}$ as well as other potential descriptor variables (table 1), we employ the Spearman rank correlation coefficient (ρ). This dimensionless measure is robust to nonlinear associations and allows comparison of variables with different units without specifying a functional relationship, as commonly applied in hydrological studies (e.g. Padrón *et al* (2017), Jehn *et al* (2020)). The aim here is to assess statistical associations rather than to develop predictive equations for ω.

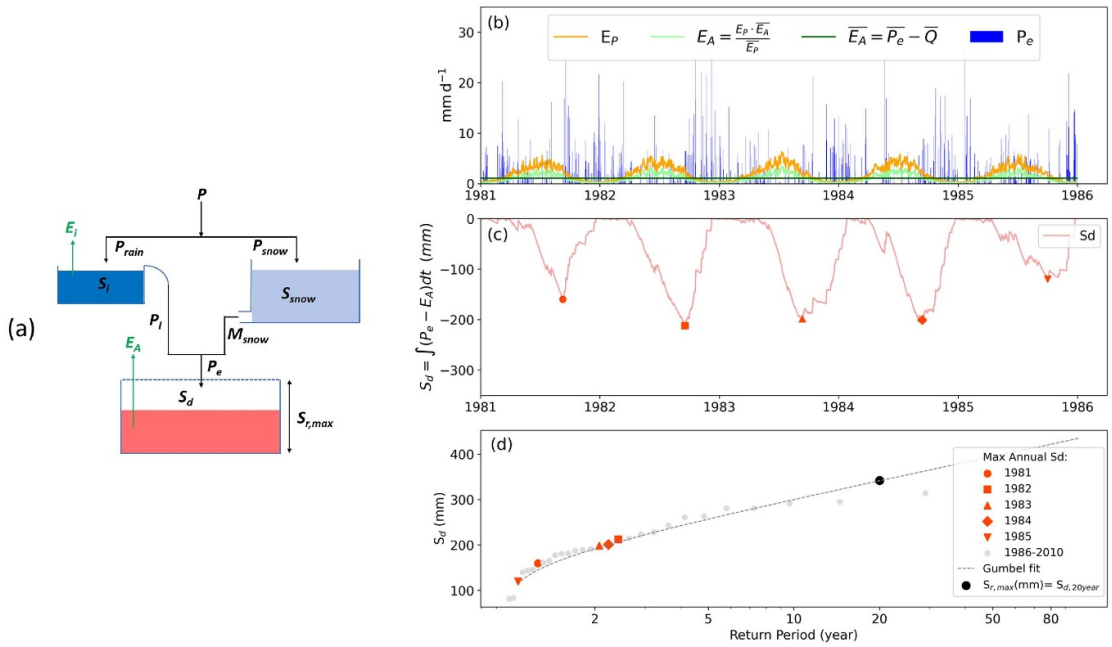

Figure 2. A schematic representation of the memory method used for calculation of $S_{r,\max}$ based on water balance data. (a) Simple water balance model representing interception and snow storages (S_i and S_{snow} respectively), used to calculate effective precipitation (P_e) by solving the water balance of interception and snow storages (for equations, see Supplement S1). (b) Time series of effective precipitation (P_e), Potential evaporation (E_P), long term average actual evaporation ($\overline{E_A}$) calculated from the long term water balance of $\overline{P_e} - \overline{Q}$, assuming negligible changes in storages over longer periods (Han *et al* 2020). Daily actual evaporation (E_A) is calculated by rescaling daily E_P with $\overline{E_A}$. (c) daily storage deficits (S_d) calculated from the cumulative difference of daily P_e—E_A, (d) Fitted Gumbel distribution to the annual maximum storage deficits S_d for different return periods and the estimated $S_{r,\max}$ that corresponds to a storage deficit with a 20 year return period. Note: panels (b) and (c) display hydroclimatic variability for 1981–1985 to avoid complexity, while panel d includes annual maximum storage deficits over a 30 year period. Red markers in panel *d* correspond to the years (1981–1985) shown in panels (b) and (c). This figure is based on synthetic data.

3. Results

For the study catchments, ω ranges from ∼1.1 to ∼14.6, with a median of ∼2.4 (figure 3(a)). Overall, 46% of catchments have ω between 2 and 3, suggesting minor deviations from the original non-parametric Budyko curve (Budyko 1974), associated with ω ∼2.6 (Greve *et al* 2015). The global distribution is skewed towards lower ω values (inset figure 3(a)), with most catchments (∼62%) below the non-parametric Budyko curve, leading to lower fractional evaporation. Spatially, ω exhibits distinct geographic patterns. In north America, particularly in eastern US, ω increases from ∼1.5 in the north to ∼3 in the south likely reflect the transition from cold to temperate climates. The central US is characterized by a north–south cluster of high ω values of >3, implying consistently high E_A/P across prairie grass- and croplands, while the western US is predominantly characterized by ω < 2.6. Along Brazil's coastline (north to south), high ω values of >3 and a distinct transition to ω as low as ∼1.5 is observed. Southern Africa and Australia are dominated by high ω clusters (>4) with median values of ∼2.6 and ∼3 respectively. In contrast, western south America exhibits ω ∼1.2–2.0. In Europe, ω varies between ∼1.5 and ∼4 except in northern Europe, where most catchments have $\omega < 2$. Similarly, most Indian catchments show lower ω values, with a few exceptions along the western and southern Coastline. Across aridity classes (inset figure 3(a)), median ω increases from humid to semi-arid regions and declines in arid regions.

Globally, $S_{r,\max}$ values varied from <10 mm in polar and cold climates to up to ∼900 mm in tropical climates with a median of 172 mm across 5717 catchments (figure 3(b)). The spatial distribution of $S_{r,\max}$ values is broadly consistent with previous regional and global studies as shown Stocker *et al* (2023) or van Oorschot *et al* (2024a). Higher $S_{r,\max}$ values between ∼300–500 mm and locally up to ∼900 mm are found in semi-humid to semi-arid regions (inset figure 3(b)) where liquid water supply is highly seasonal. For example, wide parts of the great plains region of the US are characterized by $S_{r,\max}$ values between ∼300–450 mm (median ∼350 mm). Similarly elevated $S_{r,\max}$ was found in the eastern parts of Brazil (median ∼380 mm), central Africa (albeit in a limited number of catchments), northern and western India (median ∼430 mm) and northern and western Australia (median∼380 mm). In contrast, lower $S_{r,\max}$ values <200 mm, were observed in humid and cool-temperate regions such as northern and western Europe, eastern Canada and parts of northeastern US. Overall, 60% of catchments have

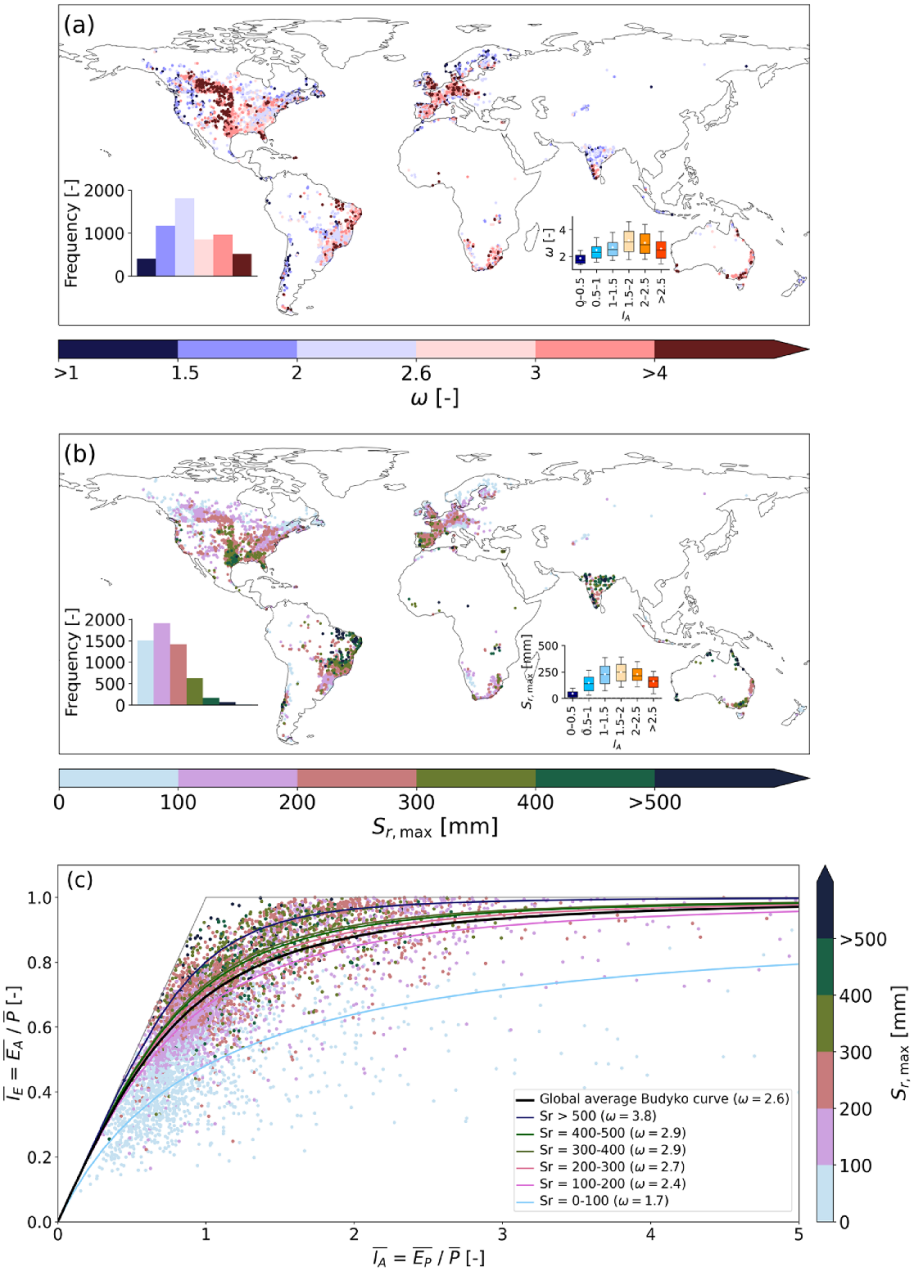

Figure 3. A) ω values calculated from equation (1) for the study catchments, based on water balance data from 1981–2010. (b) Catchment $S_{r,\max}$ values map, calculated by using memory method. Boxplot insets in panels (a) and (b) show the variation of ω and $S_{r,\max}$ respectively across different aridity index classes. The boxes represent the 25th to 75th percentiles, while whiskers extend to the 10th and 90th percentiles. Diamonds denote the arithmetic mean, and outliers are not shown. c) Catchment position in the Budyko space represented as solid circles, coloured according to the same $S_{r,\max}$ categories as in panel (b). For each $S_{r,\max}$ category, a parametric Budyko curve is fitted to the ensemble of catchments, and the corresponding ω parameter represents the best-fit for that category (not individual catchments as in panel (a)). A $\omega = 2.6$ indicates the global average Budyko curve.

$S_{r,\max}$ <200 mm indicating relatively limited root zone storage capacity.

A visual analysis shows that, overall, catchments with higher ω are associated with higher $S_{r,\max}$ values (figure 3(c)). Catchments with $S_{r,\max} \leqslant 100$ mm have $\omega \sim 1.7$, whereas catchments with $S_{r,\max} > 500$ mm, which are mostly found in sub-humid to semi-arid regions with $I_A \sim 1$–2 (inset figure 3(b)), are characterized with the highest ω values of ∼3.8. The similarity between the global spatial patterns of ω (figure 3(a)) and $S_{r,\max}$ (figures 3(b) and (c)) indicates that regions with high $S_{r,\max}$ exhibit higher ω values. This pattern highlights that an increase in $S_{r,\max}$ (figure 3(c)) tends to move catchments higher in the Budyko space reflecting a greater capacity of catchments in a given climate to partition precipitation into evaporation. This is because a higher $S_{r,\max}$ allows catchment scale vegetation to maintain root water uptake and sustain transpiration needs during periods of strong seasonal or interannual water supply

variability, thereby increasing evaporation and moving catchment higher in the Budyko space. The robust relationship between best fit ω values and $S_{r,\max}$ is quantified by a Spearman correlation with $\rho = 0.68$ ($p < 0.001$; figure 4(a)), supporting the hypothesis that $S_{r,\max}$ is a dominant driver modulating P partitioning and thus the position of individual catchments in the Budyko framework as controlled by ω.

To better explore the spatial variability of the $S_{r,\max}$–ω relationship, the global analysis was stratified into Köppen–Geiger climate zones. Unique patterns emerged in different climatic regions. In cold regions, a strong correlation with $\rho = 0.87$ ($p < 0.001$) is observed between $S_{r,\max}$ and ω (figure 4(b)), suggesting that $S_{r,\max}$ significantly influences catchment positions in the Budyko framework in these energy limited regions. Lower $S_{r,\max}$ values with a median of ∼130 mm, indicate that vegetation does not require large subsurface water volumes, consistent with low root zone storage due to limited evaporative demand and sufficient year-round water supply, aligning with generally low ω values with a median of ∼2.4 (figure 5(b)).

Catchments in the Mediterranean climate zone also exhibit a strong positive relationship between $S_{r,\max}$ and ω with $\rho = 0.83$ ($p < 0.001$; figure 4(c)) highlighting the role of $S_{r,\max}$ in buffering extended summer dry periods and modulating ω. The intermediate to high $S_{r,\max}$ values, with a median of ∼240 mm (figure 5(c)), correspond to a median ω value of ∼1.9. The less pronounced slope in the $S_{r,\max}$–ω relationship (figure 4(c)) indicates that vegetation in Mediterranean climates adapts to seasonal water availability by developing more extensive root systems to access sufficient subsurface water during dry spells to reach the same ω and thus evaporative ratios than in the cold climate zone. The strong coupling between ω and $S_{r,\max}$ further underlines that in Mediterranean climates, vegetation strongly relies on soil water storage to sustain evaporation demand during dry periods particularly in catchments with high ω values, where vegetation strongly influences precipitation partitioning through sustained access to subsurface water.

In temperate regions, a moderately strong relationship ($\rho = 0.76$; $p < 0.001$) between $S_{r,\max}$ and ω was observed (figure 4(d)). Although $S_{r,\max}$ ranging between <10 mm and ∼660 mm, its influence on ω is less pronounced than in cold and Mediterranean climates. In tropical and arid regions, the coupling between $S_{r,\max}$ and ω was significant but with $\rho = 0.64$ and 0.61, respectively, weaker compared to other regions (figures 4(e) and (f)). A weaker correlation in tropical climates, reflects that high precipitation volumes reduce the relative importance of $S_{r,\max}$ as water availability is rarely a limiting factor for evaporation. In arid regions, the weaker correlation ($\rho = 0.61$) suggests that $S_{r,\max}$ contributes to precipitation partitioning, but its influence is limited.

Its globally strong coupling with ω suggests that $S_{r,\max}$ acts as a major control on ω. To place the relative importance of this control into context of other factors that may potentially affect ω and thus the precipitation partitioning, we also analysed its relationship with 14 additional climate and landscape descriptors (table 1). Many tested variables exhibit significant, yet weaker correlations with ω (figure 6). For example, the fractions of cropland, pasture and shrubland (F_{UCPS}; $\rho = 0.33$) and forest cover (F_{Forest}; $\rho = -0.28$) exhibit only moderate correlations, while correlations with all other potential descriptors are weaker ($\rho \leqslant |0.20|$). These findings align with Padrón *et al* (2017), who reported weak correlations between ω and vegetation related variables such as forest cover, NDVI, PESWC. Among all tested variables, $S_{r,\max}$ clearly emerges as the dominant global control on ω ($\rho = 0.68$), regulating the precipitation partitioning, with similar hierarchies were found when stratified by five climate zones (supplementary figure S2).

4. Discussion

Although the ω-parameter reflects the integrated effects of all catchment characteristics next to I_{A} on partitioning (Zhang *et al* 2001), our results provide evidence for a strong global coupling between $S_{r,\max}$ and ω, underlining the dominant role of $S_{r,\max}$ in controlling the precipitation partitioning into evaporation and runoff. These findings correspond with previous studies that have demonstrated the critical role of $S_{r,\max}$ in sustaining evaporative demand across climates (Gao *et al* 2014) and ultimately controlling P partitioning within the Budyko framework. In particular, our analysis of >5000 catchments worldwide provide strong empirical support for the theoretical analysis by Porporato *et al* (2004), extending previous regional studies in Australia and the US (Donohue *et al* 2011, Gentine *et al* 2012, Daly *et al* 2019) to the global scale across a much wider spectrum of climates and landscapes.

In this study, although $S_{r,\max}$ and ω are derived from the same hydroclimatic inputs (P, Q, and E_{P}), which may introduce some non-independence, the two parameters capture distinct hydrological dynamics. $S_{r,\max}$ is based on daily storage dynamics aggregated to annual maximum deficits, whereas ω reflects the long-term (20–30 year) water balance within the Budyko framework. In other words, $S_{r,\max}$ is sensitive to intraseasonal variations in the water balance emerging from the daily interplay between water supply and demand, while ω is based exclusively on the long-term mean water balance. The robustness of the $S_{r,\max}$–ω relationship was further tested using alternative precipitation and potential evaporation datasets and multiple dataset combinations, which showed consistent relationships and preserved

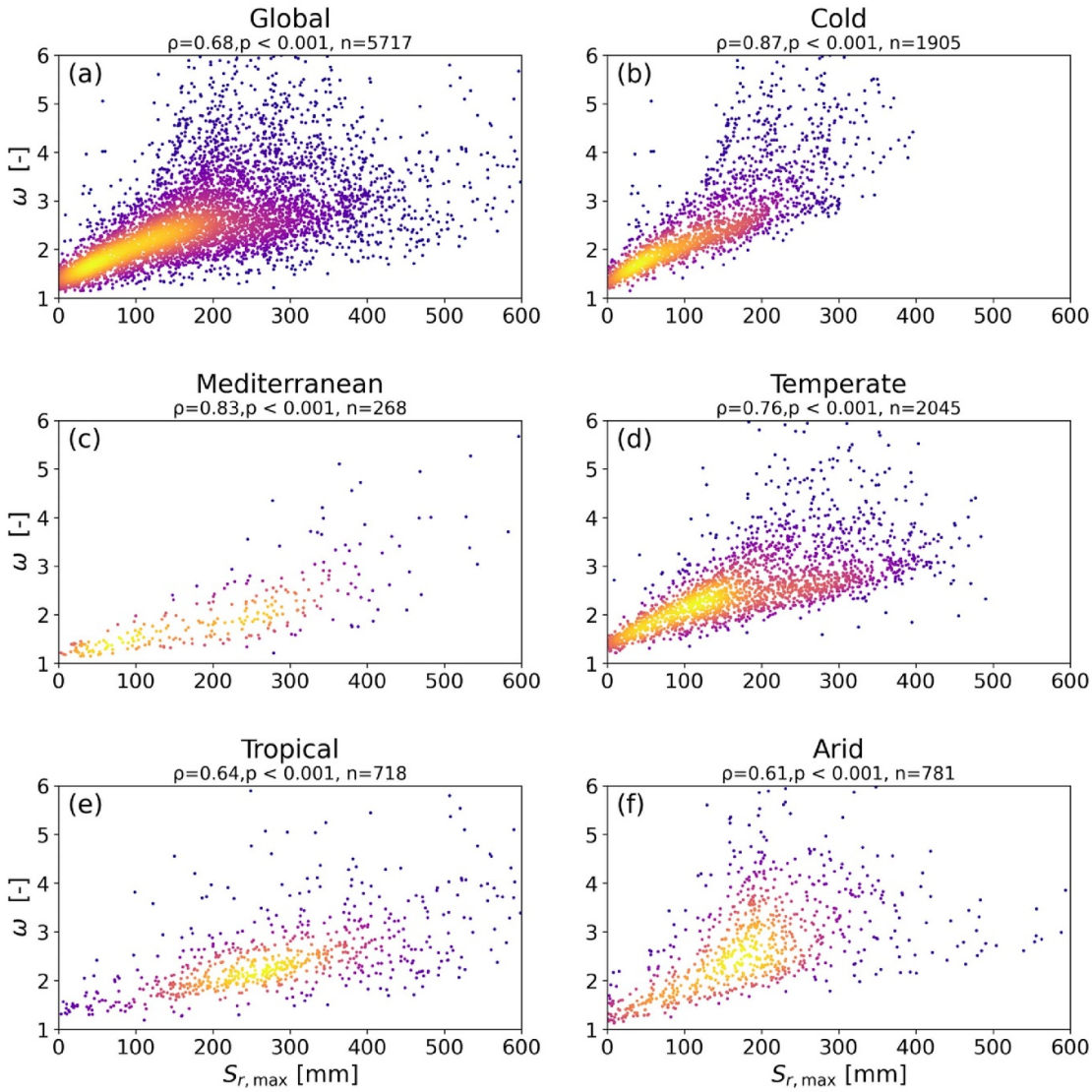

Figure 4. Spearman correlation coefficient ρ between $S_{r,\max}$ and ω for all study catchments. (a) Global scale, and (b)–(f) for the five climatic zones (see figure 1(h), based on the Köppen–Geiger classification). Each dot represents a catchment with the colour indicating point density from low (purple) to high (yellow). The Spearman correlation coefficient ρ, its p-value (whereby a value below 0.05 is often regarded as statistically significant), and number of catchments n are shown at the top of each panel. The ω and $S_{r,\max}$ values are the same as in figures 3(a) and (b) respectively, but are here separated by climate zone. Note that colours in this figure represent point density and are independent of the $S_{r,\max}$ category colours used in figures 3(a)–(c).

climate-dependent behaviour, with strongest coupling in cold regions and weakest in arid regions (figure S3). Similar results could be expected if $S_{r,\max}$ was derived from root zone observations as the robustness of memory method-based $S_{r,\max}$ estimates is supported by van Oorschot *et al* (2024a), who showed consistent correlations with root-depth and root-accessible water estimates from studies that used alternative, independent data-sources (e.g. Kleidon (2004), Schenk and Jackson (2009), Wang-Erlandsson *et al* (2016), Yang *et al* (2016b), Fan *et al* (2017), Stocker *et al* (2023)). These comparisons include the global gridded root depth dataset of Schenk and Jackson (2009), a regression-based regionalisation of rooting depth observations compiled by Schenk and Jackson (2002). While $S_{r,\max}$ is not a direct proxy for rooting depth, it represents the maximum subsurface water volume accessible to vegetation roots (van Oorschot *et al* 2024a, 2024b). The memory method is well-established and widely applied to reflect vegetation's root zone dynamics, albeit with slight differences in implementation (e.g. Donohue *et al* (2012), Gentine *et al* (2012), de Boer-euser *et al* (2016), Bouaziz *et al* (2020), McCormick *et al* (2021), Stocker *et al* (2023)). Together, these points suggest that the observed $S_{r,\max}$–ω coupling reflects a meaningful hydrological behaviour.

Similar to Padrón *et al* (2017), we find a weak global correlation between ω and PESWC ($\rho = 0.19$; figure 6) and across different climates ($\rho = -0.02$–0.38; figures S2(a)–(e)) despite its similar interpretation to $S_{r,\max}$. This weak relationship arises from the PESWC estimation method (Dunne and Willmott 2000), which uses site-specific soil water capacity

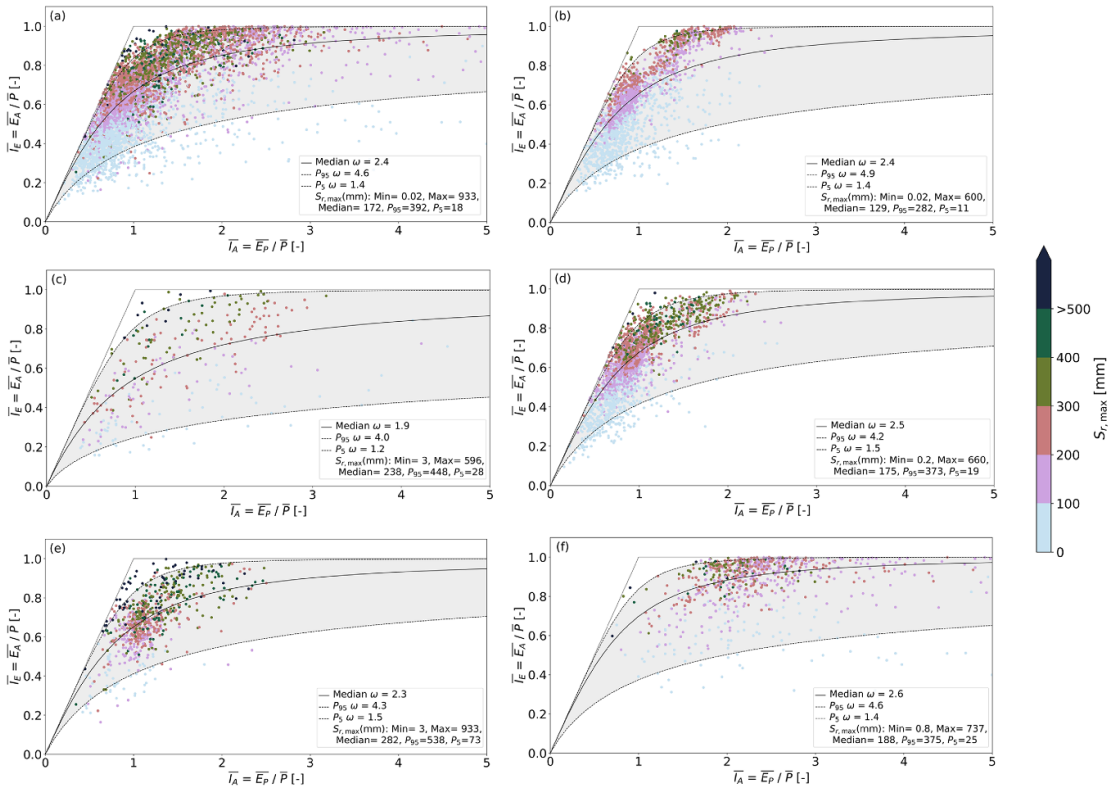

Figure 5. Catchment positions in the Budyko space, represented as solid circles, indicating $S_{r,\max}$ categories consistent with figures 3(b) and (c). Panels (a)–(f) show Budyko curves corresponding to the median, 5th percentile (P_5), and 95th percentile (P_{95}) ω values for the catchments: a) Global scale (same as figure 3(c)); (b) and (f) five climatic zones (see figure 1(h), based on Köppen–Geiger classification)—(b) cold, (c) Mediterranean, (d) temperate, (e) tropical, and (f) arid. The legend shows summary statistics of ω and $S_{r,\max}$.

integrated over average plant-specific root depths. Although theoretically correct, this approach has considerable weaknesses at catchment and global scales due to sparse root depth observations which are limited to a few thousand plants globally (e.g. Schenk and Jackson (2002)), representing the largest source of uncertainty (Dunne and Willmott 2000) and limiting the method's ability to sufficiently capture local root adaptations. Increasing evidence shows that vegetation adjusts above- and below-ground allocation to maintain water access during dry periods while sustaining competitive growth (e.g. Guswa (2008), Schymanski *et al* (2008)). In contrast, $S_{r,\max}$ is derived from observed water balance data which explicitly reflect the seasonal water–energy interplay and climatic regulation of root systems (Savenije and Hrachowitz 2017, Stocker *et al* 2023, Gao *et al* 2024). Thus $S_{r,\max}$ reflects vegetation adaptation to past climates, thereby making it more meaningful and robust descriptor of plant accessible subsurface water storage than PESWC. Although catchments may include heterogeneous land covers, memory method-based $S_{r,\max}$ represents the integrated vegetation-water interactions at the catchment scale and is therefore an appropriate functional trait for assessing controls on precipitation partitioning.

Another noteworthy result is the absence of correlation ($\rho = 0.01$, figure 6) between the Seasonality Index (I_S) of effective precipitation and ω. The $S_{r,\max}$–ω relationship versus I_S (figure 7(a)) revealed two clusters: A low I_S cluster (<0.6) indicating uniform precipitation and strong $S_{r,\max}$–ω correlation ($\rho = 0.79$), and a high I_S cluster ($\geqslant 0.6$) showing a bimodal pattern and weaker, more variable correlation ($\rho = 0.48$), suggesting that I_S modulates the $S_{r,\max}$–ω relationship. The bimodality reflects distinct hydrological processes: in cold regions (figure 7(b)) high I_S is driven by spring and early summer snowmelt aligning water supply with higher energy availability, producing proportionally higher evaporation and thus ω than regions with comparable $S_{r,\max}$, but lower I_s. In tropical regions (figure 7(e)), high I_S has an inverse effect: intense monsoon rainfall generates substantial (near-)surface runoff due to limited soil infiltration and storage, making water unavailable for vegetation (Dos Santos *et al* 2016, Yang *et al* 2016a) and leading to lower evaporation and thus ω than in regions with comparable $S_{r,\max}$ but lower I_s. Vegetation-soil interactions and interannual water storage variations further weaken the $S_{r,\max}$–ω relationship. This aligns with previous studies (Milly 1994, Porporato *et al* 2004, Hickel and Zhang 2006, Raz-Yaseef *et al* 2012,

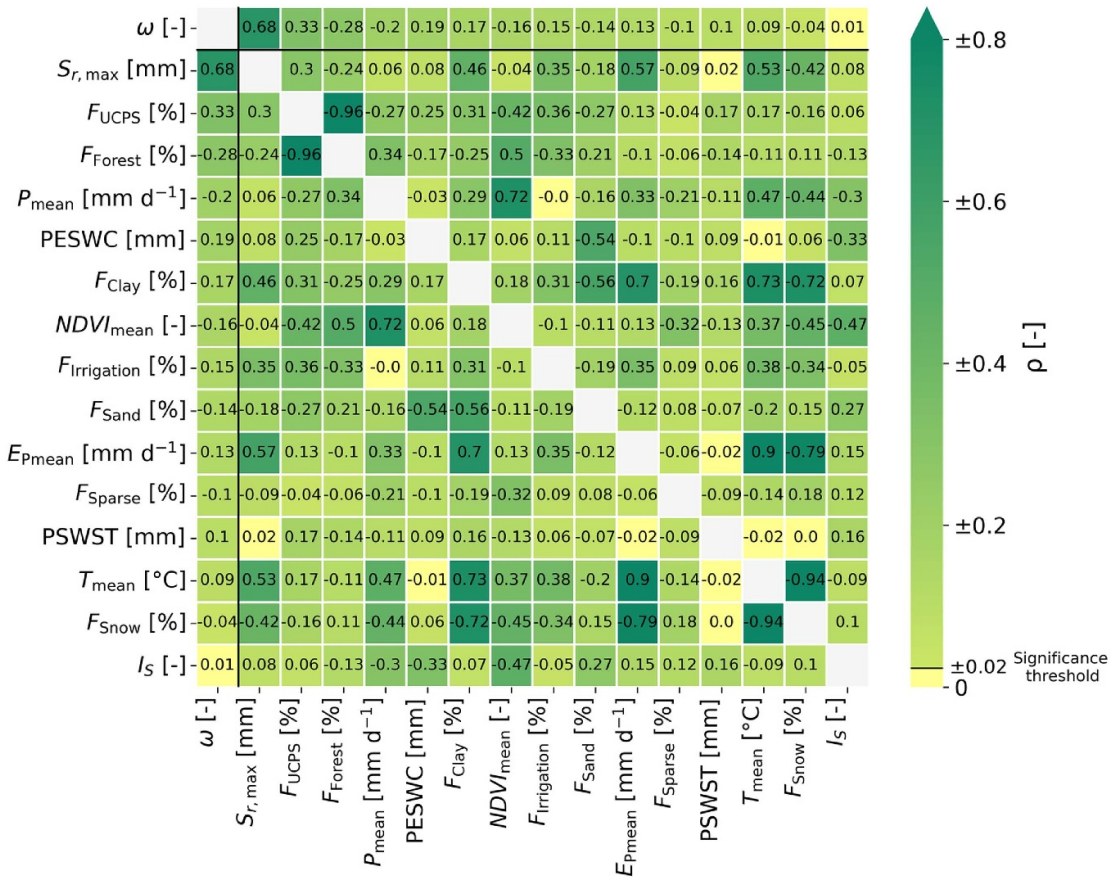

Figure 6. Spearman correlation ρ matrix between $S_{r,\max}$, ω and other potential explanatory variables as detailed in table 1. Black lines highlight correlations between ω and all other variables. Correlations with $|\rho|$ values below the marked threshold (∼0.02) are not statistically significant at the 5% level.

Berghuijs *et al* 2014) suggesting that precipitation seasonality can modulate P partitioning differently across timescales.

The reduced $S_{r,\max}$–ω coupling in arid climates (figure 4(f)) is linked to patchy, low-density vegetation in deserts (e.g. Northern Chile, Southwestern US) and differences in vegetation composition and water management strategies. For example, prairie and steppe grasses in the central US and Central Asia (Ke *et al* 2012) go dormant during dry periods, reducing water use and resulting in $S_{r,\max} < 200$ mm (figures 3(b) and S4) and low ω values (figure 3(a)). In contrast, Caatinga shrublands in North–Eastern Brazil with succulent species (Goldstein and DellaSala 2020), and deep-rooted Eucalyptus in Australia (Booth and Muir 2020) have higher $S_{r,\max}$ (figures 3(b) and S4). This vegetation adaptation variability is reflected in two divergent patterns (i.e. lower and upper envelopes) in the $S_{r,\max}$–ω relationship within arid zones (figures 4(f) and S4), representing hot-arid and cool-arid regions, respectively. Lower-envelope (hot-arid) catchments require higher $S_{r,\max}$ for the same ω due to higher evaporative demand, whereas upper-envelope (cool-arid) catchments can proportionally evaporate at different levels with much lower $S_{r,\max}$. These contrasting behaviours align with temperature and rainfall intensity gradients (figures S5(a) and (b)), suggesting two distinct vegetation water-use strategies within arid regions.

Additionally, weaker $S_{r,\max}$–ω correlations in arid and tropical regions ($\rho = 0.61$–0.64; figures 4(e) and (f)) may result from uncertainties in P, Q, and E_P estimates, which are higher in these regions due to sparse gauge coverage and challenges in estimating E_p (Sheffield *et al* 2006, Mueller *et al* 2011), thereby increasing noise in forcing data and reducing correlation strength. However, giving the ecological variability discussed above, these patterns are unlikely to arise exclusively from data noise. Instead, our results suggest ecological adaptations are the main driver: in many arid catchments—such as in India and north-eastern Brazil—woody and shrub vegetation develop deeper or lateral opportunistic roots to survive seasonal or multi-year droughts (Canadell *et al* 1996, Schenk and Jackson 2002, Fan *et al* 2017), resulting in $S_{r,max}$ values comparable to other climatic zones (figures 3(b) and S4). Thus, weaker correlations reflect a combination of data uncertainty and ecological variability, rather than solely ecological or noise-related effects.

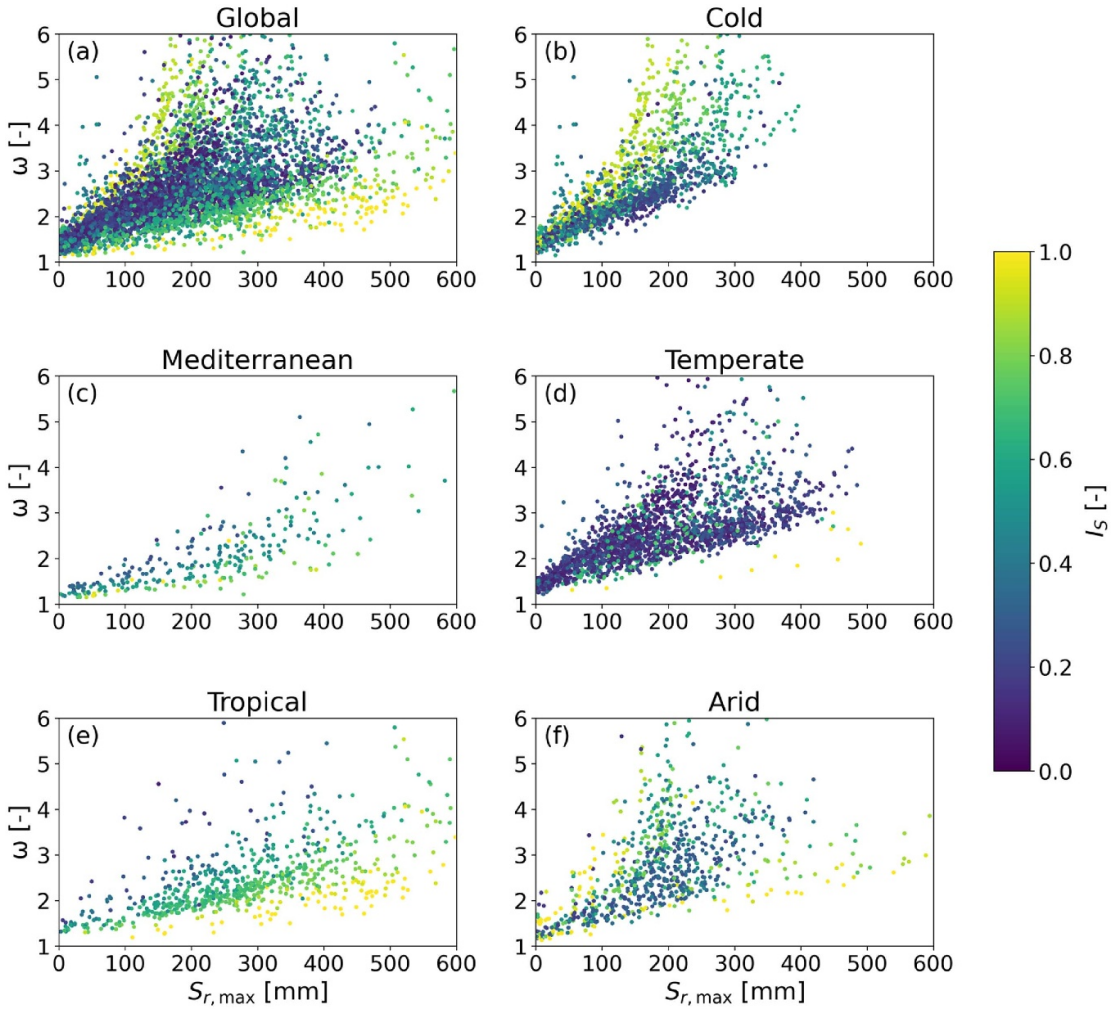

Figure 7. Relationship between $S_{r,\max}$ and ω values: (a) global scale; (b)–(f) five climatic zones: (b) cold, (c) Mediterranean, (d) temperate, (e) tropical, and (f) arid. Each dot represents a catchment with the colour indicating seasonality index of effective precipitation I_S.

The results align with a broader resurgence of top–down models in environmental science that capture and describe emergent hydrological–ecological behaviour in tractable ways. In this context, an advantage of the Budyko framework is its simplicity and robustness, which allows for mechanistically plausible interpretation of the ω-parameter and its coupling with dominant controls such as $S_{r,\max}$. As a defining feature, emergent behaviour does not only aggregate smaller-scale behaviour, but, critically, also implicitly account for feedbacks between individual smaller-scale system component. Such a representation of feedback is unlikely to be achieved with more complex bottom–up models which would require thus far unknown feedbacks to be hardcoded into individual components. This approach enables deeper insights, which are ultimately instrumental for a better process representation in more complex hydrological, land surface models and eventually Earth system models (ESMs). Recent studies show that climate-controlled root zone parameters improve water flux simulations in land surface (van Oorschot *et al* 2021) and hydrological models (de Boer-euser *et al* 2016), particularly for systems under change (e.g. Bouaziz *et al* (2022), Tempel *et al* (2024), Ponds *et al* (2025)). These findings highlight the potential for incorporating such aggregated metrics into model frameworks. It is therefore to be expected that the observed $S_{r,\max}$–ω relationship may similarly serve as an emergent constraint (Hall *et al* 2019) for ESMs, where considerable uncertainty remains in representing root-zone processes. Thus, Budyko-type approaches not only advance conceptual understanding but also provide potential new pathways towards more robustly constraining land components of ESMs.

A further insight from our results is that the maximum $S_{r,\max}$ values (∼450–800 mm) (Gao *et al* 2014, Singh *et al* 2020, van Oorschot *et al* 2024b) are not arbitrary, but governed by physical limits of water and energy partitioning. Within Budyko space, catchments with high $S_{r,\max}$ also exhibit high ω, operating close to these limits. Thus, the Budyko

space and its limits (figure 3(c)) provide a theoretical basis for the upper limits of $S_{r,\max}$. Higher $S_{r,\max}$ values were observed in semi-humid (I_A = 1.0–1.5; median ~230 mm) to semi-arid regions (I_A = 1.5–2.0; median ~250) rather than in arid regions ($I_A > 2$; median ~165 mm) (inset of figure 3(b)), aligning with previous studies linking these values to vegetation adaptations for maximizing subsurface water access. Vegetation in semi-humid to semi-arid regions, which show the highest $S_{r,\max}$, tends to develop more extensive root systems vertically, laterally and/or density-wise to access subsurface water to compensate for seasonal fluctuations (Gentine *et al* 2012, Fan *et al* 2017, Singh *et al* 2020).

5. Conclusions

In this study, we tested the hypothesis that root zone storage capacity ($S_{r,\max}$) controls precipitation partitioning through its coupling with the ω-parameter. $S_{r,\max}$, the maximum subsurface water accessible to vegetation roots, was estimated using the Memory Method for 5717 river catchments across diverse climatic regions. Globally, a significant correlation ($\rho = 0.68$) was found between $S_{r,\max}$ and ω. Stratified analysis by climatic zones further revealed that $S_{r,\max}$ has strongest influence on P partitioning in cold ($\rho = 0.87$) and Mediterranean ($\rho = 0.83$) regions followed by temperate ($\rho = 0.76$), tropical ($\rho = 0.64$) and arid climates ($\rho = 0.61$). Analysing other variables that may explain spatial variations in ω, $S_{r,\max}$ exhibited the strongest and most consistent correlation with ω, providing empirical support that it is the dominant global control on precipitation partitioning. As a measure that explicitly integrates the combined influences of the seasonal signals of water supply and atmospheric water demand, regional differences in $S_{r,\max}$ indicate that, at a given aridity, precipitation partitioning E_A/P is largely a manifestation of vegetation adaptation to the interplay between these seasonal signals. Our results further suggest that the Budyko framework provides a theoretical basis for the maximum values of $S_{r,max}$ observed in nature, constrained by the water and energy limits. The $S_{r,\max}$–ω relationship may therefore serve as a simple, aggregated constraint for ESMs. This highlights that $S_{r,\max}$ is not only a key factor for precipitation partitioning but also fundamentally limited by the same principles that govern the Budyko curve.

Acknowledgment

This research has been supported by the Higher Education Commission of Pakistan (Grant No. Ref:1(2)/HRD/OSSIII/2021/HEC/19607).

Data availability statement

Daily precipitation and temperature data were obtained from the GSWP-3 dataset, accessible at https://doi.org/10.48364/ISIMIP.886955 (Dirmeyer *et al* 2006, Lange and Büchner 2020). Streamflow data was obtained from multiple sources: GSIM data from https://doi.org/10.1594/PANGAEA.887477 (Do *et al* 2018) and https://doi.org/10.1594/PANGAEA.887470 (Gudmundsson *et al* 2018); Caravan data from https://zenodo.org/records/14673536 (Kratzert *et al* 2023); African catchments data from https://doi.org/10.23708/LXGXQ9 (Tramblay *et al* 2021); and Central Asian catchments data from https://zenodo.org/records/8147591 (Marti *et al* 2023).

Supplementary data consisting of climatic and topographic characteristics of 5717 study catchments is available at https://doi.org/10.5281/zenodo.15783320 (Ibrahim *et al* 2025b).

Supplement available at http://doi.org/10.1088/1748-9326/ae612a/data1.

ORCID iDs

Muhammad Ibrahim 0009-0005-9147-5953
Fransje van Oorschot 0000-0002-8811-0620
Ruud van der Ent 0000-0001-5450-4333
Markus Hrachowitz 0000-0003-0508-1017
Miriam Coenders-Gerrits 0000-0002-7340-4685

References

Beck H E, Zimmermann N E, McVicar T R, Vergopolan N, Berg A and Wood E F 2018 Present and future Koppen-Geiger climate classification maps at 1-km resolution *Sci. Data* **5** 180214

Berghuijs W R, Sivapalan M, Woods R A and Savenije H H G 2014 Patterns of similarity of seasonal water balances: a window into streamflow variability over a range of time scales *Water Resour. Res.* **50** 5638–61

Booth T H and Muir P R 2020 Climate change impacts on Australia's eucalypt and coral species: comparing and sharing knowledge across disciplines *WIREs Clim. Change* **11** e657

Bouaziz L J E, Aalbers E E, Weerts A H, Hegnauer M, Buiteveld H, Lammersen R, Stam J, Sprokkereef E, Savenije H H G and Hrachowitz M 2022 Ecosystem adaptation to climate change: the sensitivity of hydrological predictions to time-dynamic model parameters *Hydrol. Earth Syst. Sci.* **26** 1295–318

Bouaziz L J E, Steele-Dunne S C, Schellekens J, Weerts A H, Stam J, Sprokkereef E, Winsemius H H C, Savenije H H G and Hrachowitz M 2020 Improved understanding of the link between catchment-scale vegetation accessible storage and satellite-derived soil water index *Water Resour. Res.* **56** e2019WR026365

Bouaziz L, Weerts A, Schellekens J, Sprokkereef E, Stam J, Savenije H and Hrachowitz M 2018 Redressing the balance: quantifying net intercatchment groundwater flows *Hydrol. Earth Syst. Sci.* **22** 6415–34

Budyko M I 1974 *Climate and Life* (Academic)
Budyko 1948 *Isparenie V Estestvennykh Usloviyakh [Evaporation under Natural Conditions]* (Gidrometeoizdat)
Canadell J, Jackson R B, Ehleringer J, Mooney H A, Sala O E and Schulze E-D 1996 Maximum rooting depth of vegetation types at the global scale *Oecologia* **108** 583–95
Choudhury B 1999 Evaluation of an empirical equation for annual evaporation using field observations and results from a biophysical model *J. Hydrol.* **216** 99–110
Daly E, Calabrese S, Yin J and Porporato A 2019 Hydrological spaces of long-term catchment water balance *Water Resour. Res.* **55** 10747–64
de Boer-euser T, McMillan H K, Hrachowitz M, Winsemius H C and Savenije H H G 2016 Influence of soil and climate on root zone storage capacity *Water Resour. Res.* **52** 2009–24
Dirmeyer P A, Gao X, Zhao M, Guo Z, Oki T and Hanasaki N 2006 GSWP-2: multimodel analysis and implications for our perception of the land surface *Bull. Am. Meteorol. Soc.* **87** 1381–98
Do H X, Gudmundsson L, Leonard M and Westra S 2018 The global streamflow indices and metadata archive (GSIM)—part 1: the production of a daily streamflow archive and metadata *Earth Syst. Sci. Data* **10** 765–85
Donohue R J, Roderick M L and McVicar T R 2011 Assessing the differences in sensitivities of runoff to changes in climatic conditions across a large basin *J. Hydrol.* **406** 234–44
Donohue R J, Roderick M L and McVicar T R 2012 Roots, storms and soil pores: incorporating key ecohydrological processes into Budyko's hydrological model *J. Hydrol.* **436–437** 35–50
Donohue R, Roderick M and McVicar T R 2007 On the importance of including vegetation dynamics in Budyko's hydrological model *Hydrol. Earth Syst. Sci.* **11** 983–95
Dos Santos J C N, de Andrade E M, Medeiros P H A, Guerreiro M J S and de Queiroz Palácio H A 2016 Effect of rainfall characteristics on runoff and water erosion for different land uses in a tropical semiarid region *Water Resour. Manage.* **31** 173–85
Dralle D N, Jesse Hahm W, Rempe D M, Karst N, Anderegg L D L, Thompson S E, Dawson T E and Dietrich W E 2020 Plants as sensors: vegetation response to rainfall predicts root-zone water storage capacity in Mediterranean-type climates *Environ. Res. Lett.* **15** 104074
Dunne K A and Willmott C J 2000 *Global Distribution of Plant-Extractable Water Capacity of Soil (Dunne)* (ORNL Distributed Active Archive Center) (https://doi.org/10.3334/ORNLDAAC/545)
Fan Y, Miguez-Macho G, Jobbagy E G, Jackson R B and Otero-Casal C 2017 Hydrologic regulation of plant rooting depth *Proc. Natl Acad. Sci. USA* **114** 10572–7
Fu B P 1981 On the calculation of the evaporation from land surface *Sci. Atmos. Sin* **5** 23–31
Gao H, Hrachowitz M, Schymanski S J, Fenicia F, Sriwongsitanon N and Savenije H H G 2014 Climate controls how ecosystems size the root zone storage capacity at catchment scale *Geophys. Res. Lett.* **41** 7916–23
Gao H, Hrachowitz M, Wang-Erlandsson L, Fenicia F, Xi Q, Xia J, Shao W, Sun G and Savenije H H G 2024 Root zone in the Earth system *Hydrol. Earth Syst. Sci.* **28** 4477–99
Gentine P, D'Odorico P, Lintner B R, Sivandran G and Salvucci G 2012 Interdependence of climate, soil, and vegetation as constrained by the Budyko curve *Geophys. Res. Lett.* **39** L19404
Ghiggi G, Humphrey V, Seneviratne S I and Gudmundsson L 2019 GRUN: an observation-based global gridded runoff dataset from 1902 to 2014 *Earth Syst. Sci. Data* **11** 1655–74
Goldstein M I and DellaSala D A 2020 *Encyclopedia of the World's Biomes* (Elsevier)
Greve P, Gudmundsson L, Orlowsky B and Seneviratne S I 2015 Introducing a probabilistic Budyko framework *Geophys. Res. Lett.* **42** 2261–9
Gudmundsson L, Do H X, Leonard M and Westra S 2018 The global streamflow indices and metadata archive (GSIM)—part 2: quality control, time-series indices and homogeneity assessment *Earth Syst. Sci. Data* **10** 787–804
Guswa A J 2008 The influence of climate on root depth: a carbon cost-benefit analysis *Water Resour. Res.* **44** W02427
Hall A, Cox P, Huntingford C and Klein S 2019 Progressing emergent constraints on future climate change *Nat. Clim. Change* **9** 269–78
Han J, Yang Y, Roderick M L, McVicar T R, Yang D, Zhang S and Beck H E 2020 Assessing the steady-state assumption in water balance calculation across global catchments *Water Resour. Res.* **56** e2020WR027392
Hargreaves G H and Samani Z A 1982 Estimating potential evapotranspiration *J. Irrig. Drain. Div.* **108** 225–30
Hengl T *et al* 2017 SoilGrids250m: global gridded soil information based on machine learning *PLoS One* **12** e0169748
Hickel K and Zhang L 2006 Estimating the impact of rainfall seasonality on mean annual water balance using a top-down approach *J. Hydrol.* **331** 409–24
Hou Y, Guo H, Yang Y and Liu W 2022 Global evaluation of runoff simulation from climate, hydrological and land surface models *Water Resour. Res.* **59** e2021WR031817
Hrachowitz M, Stockinger M, Coenders-Gerrits M, van der Ent R, Bogena H, Lücke A and Stumpp C 2021 Reduction of vegetation-accessible water storage capacity after deforestation affects catchment travel time distributions and increases young water fractions in a headwater catchment *Hydrol. Earth Syst. Sci.* **25** 4887–915
Ibrahim M, Coenders M, Van der Ent R and Markus Hrachowitz M 2025a Catchments do not strictly follow Budyko curves over multiple decades but deviations are minor and predictable *Hydrol. Earth Syst. Sci.* **29** 1703–23
Ibrahim M, Coenders M, Van der Ent R and Markus Hrachowitz M 2025b *Supplement data: Catchment precipitation partitioning in the Budyko framework is controlled by root zone storage capacity [Data set]* Zenodo (https://doi.org/10.5281/zenodo.15783320)
Jaramillo F and Destouni G 2015 Local flow regulation and irrigation raise global human water consumption and footprint *Science* **350** 1248–51
Jaramillo F, Piemontese L, Berghuijs W R, Wang-Erlandsson L, Greve P and Wang Z 2022 Fewer basins will follow their Budyko curves under global warming and fossil-fueled development *Water Resour. Res.* **58** e2021WR031825
Jehn F U, Bestian K, Breuer L, Kraft P and Houska T 2020 Using hydrological and climatic catchment clusters to explore drivers of catchment behavior *Hydrol. Earth Syst. Sci.* **24** 1081–100
Ke Y, Leung L R, Huang M, Coleman A M, Li H and Wigmosta M S 2012 Development of high resolution land surface parameters for the community land model *Geosci. Model Dev.* **5** 1341–62
Kleidon A 2004 Global datasets of rooting zone depth inferred from inverse methods *J. Clim.* **17** 2714–22
Kratzert F *et al* 2023 Caravan—a global community dataset for large-sample hydrology *Sci. Data* **10** 61
Laio F, Porporato A, Ridolfi L and Rodriguez-Iturbe I 2001 Plants in water-controlled ecosystems: active role in hydrologic processes and response to water stress: II. Probabilistic soil moisture dynamics *Adv. Water Resour.* **24** 707–23
Lange S and Büchner M 2020 ISIMIP2a atmospheric climate input data (https://doi.org/10.48364/ISIMIP.886955)
Li D, Pan M, Cong Z, Zhang L and Wood E 2013 Vegetation control on water and energy balance within the Budyko framework *Water Resour. Res.* **49** 969–76
Li Z and Quiring S M 2022 Projection of streamflow change using a time-varying Budyko framework in the contiguous United States *Water Resour. Res.* **58** e2022WR033016
Marti B, Yakovlev A, Karger D N, Ragettli S, Zhumabaev A, Wakil A W and Siegfried T 2023 CA-discharge: geo-located discharge time series for mountainous rivers in central Asia *Sci. Data* **10** 579
McCormick E L, Dralle D N, Hahm W J, Tune A K, Schmidt L M, Chadwick K D and Rempe D M 2021 Widespread woody

plant use of water stored in bedrock *Nature* **597** 225–9
Mezentsev V J 1955 More on the calculation of average total evaporation *Meteorol. Gidrol.* **5** 24–26
Mianabadi A, Davary K, Pourreza-Bilondi M and Coenders-Gerrits A M J 2020 Budyko framework; towards non-steady state conditions *J. Hydrol.* **588** 125089
Milly P 1993 An analytic solution of the stochastic storage problem applicable to soil water *Water Resour. Res.* **30** 3755–8
Milly P 1994 Climate, soil water storage, and the average annual water balance *Water Resour. Res.* **30** 2143–56
Mueller B *et al* 2011 Evaluation of global observations-based evapotranspiration datasets and IPCC AR4 simulations *Geophys. Res. Lett.* **38** L06402
Nijzink R *et al* 2016 The evolution of root-zone moisture capacities after deforestation: a step towards hydrological predictions under change? *Hydrol. Earth Syst. Sci.* **20** 4775–99
Oldekop E 1911 Evaporation from the surface of river basins (Испареніе съ поверхности рѣчныхъ бассейновъ) *Collection of the Works of Students of the Meteorological Observatory* (University of Tartu-Jurjew-Dorpat Tartu)
Padrón R S, Gudmundsson L, Greve P and Seneviratne S I 2017 Large-scale controls of the surface water balance over land: insights from a systematic review and meta-analysis *Water Resour. Res.* **53** 9659–78
Pinzon J E, Pak E W, Tucker C J, Bhatt U S, Frost G V and Macander M J 2023 Global vegetation greenness (NDVI) from AVHRR GIMMS-3G+, 1981–2022 (https://doi.org/10.3334/ORNLDAAC/2187)
Ponds M, Hanus S, Zekollari H, ten Veldhuis M-C, Schoups G, Kaitna R and Hrachowitz M 2025 Adaptation of root zone storage capacity to climate change and its effects on future streamflow in Alpine catchments: towards non-stationary model parameters *Hydrol. Earth Syst. Sci.* **29** 3545–68
Porporato A, Daly E and Rodriguez-Iturbe I 2004 Soil water balance and ecosystem response to climate change *Am. Nat.* **164** 625–32
Potter N J, Zhang L, Milly P C D, McMahon T A and Jakeman A J 2005 Effects of rainfall seasonality and soil moisture capacity on mean annual water balance for Australian catchments *Water Resour. Res.* **41** W06007
Raz-Yaseef N, Yakir D, Schiller G and Cohen S 2012 Dynamics of evapotranspiration partitioning in a semi-arid forest as affected by temporal rainfall patterns *Agric. For. Meteorol.* **157** 77–85
Reaver N G F, Kaplan D A, Klammler H and Jawitz J W 2022 Theoretical and empirical evidence against the Budyko catchment trajectory conjecture *Hydrol. Earth Syst. Sci.* **26** 1507–25
Savenije H H G and Hrachowitz M 2017 HESS opinions catchments as meta-organisms—a new blueprint for hydrological modelling *Hydrol. Earth Syst. Sci.* **21** 1107–16
Schenk H J and Jackson R B 2002 Rooting depths, lateral root spreads and below-ground/above-ground allometries of plants in water-limited ecosystems *J. Ecol.* **90** 480–94
Schenk H and Jackson R 2009 Islscp ii ecosystem rooting depths *ORNL Distributed Active Archive Center (DAAC) dataset 10.3334/ORNLDAAC/929 (2009*, 929)
Schreiber P 1904 Über die Beziehungen zwischen dem Niederschlag und der Wasserführung der Flüsse in Mitteleuropa *Z. Meteorol.* **21** 441–52
Schymanski S J, Sivapalan M, Roderick M L, Beringer J and Hutley L B 2008 An optimality-based model of the coupled soil moisture and root dynamics *Hydrol. Earth Syst. Sci.* **12** 913–32
Shao Q, Traylen A and Zhang L 2012 Nonparametric method for estimating the effects of climatic and catchment characteristics on mean annual evapotranspiration *Water Resour. Res.* **48** W03517
Sheffield J, Goteti G and Wood E F 2006 Development of a 50-year high-resolution global dataset of meteorological forcings for land surface modeling *J. Clim.* **19** 3088–111
Siebert S, Kummu M, Porkka M, Döll P, Ramankutty N and Scanlon B R 2015 A global data set of the extent of irrigated land from 1900 to 2005 *Hydrol. Earth Syst. Sci.* **19** 1521–45
Singh C, Wang-Erlandsson L, Fetzer I, Rockström J and van der Ent R 2020 Rootzone storage capacity reveals drought coping strategies along rainforest-savanna transitions *Environ. Res. Lett.* **15** 124021
Stacke T and Hagemann S 2021 HydroPy (v1.0): a new global hydrology model written in Python *Geosci. Model Dev.* **14** 7795–816
Sterling S M, Ducharne A and Polcher J 2012 The impact of global land-cover change on the terrestrial water cycle *Nat. Clim. Change* **3** 385–90
Stocker B D, Tumber-Davila S J, Konings A G, Anderson M C, Hain C and Jackson R B 2023 Global patterns of water storage in the rooting zones of vegetation *Nat. Geosci.* **16** 250–6
Tempel N T, Bouaziz L, Taormina R, van Noppen E, Stam J, Sprokkereef E and Hrachowitz M 2024 Catchment response to climatic variability: implications for root zone storage and streamflow predictions *Hydrol. Earth Syst. Sci.* **28** 4577–97
Tixeront J 1964 Prévision des apports des cours d'eau *Publication de l'Association Int.e D'hydrologie Scientifique* pp 118–26
Tramblay Y *et al* 2021 ADHI: the African database of hydrometric indices (1950–2018) *Earth Syst. Sci. Data* **13** 1547–60
Turc L 1954 Le bilan d'eau des sols: relation entre la precipitations, l'evaporation et l'ecoulement *Ann. Agron. A* **5** 491–596
van Oorschot F, Hrachowitz M, Viering T, Alessandri A and van der Ent R J 2024a The global patterns in vegetation accessible subsurface water storage emerge from spatially varying importance of individual drivers *Environ. Res. Lett.* **19** 124018
van Oorschot F, van der Ent R J, Alessandri A and Hrachowitz M 2024b Influence of irrigation on root zone storage capacity estimation *Hydrol. Earth Syst. Sci.* **28** 2313–28
van Oorschot F, van der Ent R J, Hrachowitz M and Alessandri A 2021 Climate-controlled root zone parameters show potential to improve water flux simulations by land surface models *Earth Syst. Dyn.* **12** 725–43
Wang D and Hejazi M 2011 Quantifying the relative contribution of the climate and direct human impacts on mean annual streamflow in the contiguous United States *Water Resour. Res.* **47** W00J12
Wang S, Hrachowitz M and Schoups G 2024 Multi-decadal fluctuations in root zone storage capacity through vegetation adaptation to hydro-climatic variability have minor effects on the hydrological response in the Neckar river basin, Germany *Hydrol. Earth Syst. Sci.* **28** 4011–33
Wang-Erlandsson L, Bastiaanssen W G M, Gao H, Jägermeyr J, Senay G B, van Dijk A I J M, Guerschman J P, Keys P W, Gordon L J and Savenije H H G 2016 Global root zone storage capacity from satellite-based evaporation *Hydrol. Earth Syst. Sci.* **20** 1459–81
Webb R, Rosenzweig C E and Levine E R 2000 Global soil texture and derived water-holding capacities (Webb *et al*) (https://doi.org/10.3334/ORNLDAAC/548)
Williams C A *et al* 2012 Climate and vegetation controls on the surface water balance: synthesis of evapotranspiration measured across a global network of flux towers *Water Resour. Res.* **48** W06523
Winkler K, Fuchs R, Rounsevell M and Herold M 2021 Global land use changes are four times greater than previously estimated *Nat. Commun.* **12** 2501
Xu X, Liu W, Scanlon B R, Zhang L and Pan M 2013 Local and global factors controlling water-energy balances within the Budyko framework *Geophys. Res. Lett.* **40** 6123–9
Yang T, Wang Q, Su L, Wu L, Zhao G, Liu Y and Zhang P 2016a An approximately semi-analytical model for describing surface runoff of rainwater over sloped land *Water Resour. Manage.* **30** 3935–48

Yang Y, Donohue R J and McVicar T R 2016b Global estimation of effective plant rooting depth: implications for hydrological modeling *Water Resour. Res.* **52** 8260–76

Zhang L, Dawes W R and Walker G R 2001 Response of mean annual evapotranspiration to vegetation changes at catchment scale *Water Resour. Res.* **37** 701–8

Zhang L, Hickel K, Dawes W R, Chiew F H S, Western A W and Briggs P R 2004 A rational function approach for estimating mean annual evapotranspiration *Water Resour. Res.* **40** W02502

Zhou G *et al* 2015 Global pattern for the effect of climate and land cover on water yield *Nat. Commun.* **6** 5918